Optical Fiber Technology 30 (2016) 184–189

Contents lists available at ScienceDirect

Optical Fiber Technology

www.elsevier.com/locate/yofte

Regular Articles

A circular photonic crystal fiber supporting 26 OAM modes

Wei Tian [a], Hu Zhang [a,b], Xiaoguang Zhang [a,*], Lixia Xi [a], Wenbo Zhang [c], Xianfeng Tang [a]

[a] State Key Laboratory of Information Photonics and Optical Communications, Beijing University of Posts and Telecommunications, Beijing 100876, China
[b] School of Ethnic Minority Education, Beijing University of Posts and Telecommunications, Beijing 100876, China
[c] School of Science, Beijing University of Posts and Telecommunications, Beijing 100876, China

ARTICLE INFO

Article history:
Received 26 May 2016
Revised 12 July 2016
Accepted 22 July 2016

Keywords:
Orbital angular momentum
Circular photonic crystal fiber
Fiber design
Fiber optics communication

ABSTRACT

A new design of a circular photonic crystal fiber, which can support 26 OAM modes, is proposed. The numerical analysis shows that the proposed fiber possesses very good values of the fiber parameters, such as low confinement loss which is lower than 0.003 dB/m at wavelength of 1.55 μm, flat chromatic dispersion whose dispersion variation for the OAM modes with the order number $|l| \leqslant 4$ is within 39.84 ps/nm/km over a 750 nm bandwidth from 1.25 to 2 μm, and small nonlinear coefficient which is less than 2.08 W^{-1}/km for all modes at 1.55 μm. In addition, the influence of geometric deformation on the modal birefringence of the proposed fiber has also been discussed. It is proved that the modal birefringence caused by the geometric deformation is different for different vector modes, and most of the higher order modes have a smaller modal birefringence than the lower order modes when the ellipticity is less than 1.08.

1. Introduction

Orbital angular momentum (OAM) can be another dimension for multiplexing. The orthogonality between any two OAM modes and its theoretically infinite states of the modes (its topological charge l can take any positive and negative integers except 0) make OAM multiplexing to be one of the promising candidates of space division multiplexing [1–5]. Unfortunately, the traditional step-index multimode fiber cannot well support stable OAM mode transmission. So, it is important to design the special optical fibers which can support OAM mode transmission.

So far, many kinds of special fibers which can support the transmission of OAM modes have been proposed, such as spun fiber [6], ring fiber [7–10], air-core fiber [11], twisted air-core fiber [12], inverse-parabolic graded-index profile fiber [13], trench-assisted ring fiber [14] and the new multi-orbital-angular-momentum multi-core supermode fiber (MOMCSF) [15], and so on.

The fibers in which the OAM modes can propagate should possess low loss, relatively flat dispersion coefficient, large effective area, and especially the high refractive index contrast between the mode transmission region and cladding to ensure the transmitting OAM modes not to couple into LP modes [10]. The OAM fibers proposed in the literature mentioned above do not have enough parameters to be adjusted to ensure the good features for OAM modes mentioned above, and most of them need to be doped accurately [10,11,16,17]. In 2012, Yang Yue et al. firstly proposed that we can use the photonic crystal fiber to support the transmission of the OAM modes [18]. The designed ring PCF uses As_2S_3 and air holes to realize the large material index contrast, but it can only support 2 OAM ($l = \pm 1$) modes and has a larger dispersion. In addition, there are also other kinds of PCF which can be used to support OAM modes, such as multicore photonic crystal fiber [19] and twisted photonic crystal fiber [20]. In this paper, we propose a new circular photonic crystal fiber (C-PCF) whose shape has a central air hole and several outer air-hole rings with a ring region to hold 26 OAM modes working at the wavelength range from 1.25 to 1.9 μm (650 nm). The new C-PCF needs no doping and it has more adjustable parameters.

In [21] Gai Zhou et al. independently proposed a microstructure ring fiber whose structure seems similar to the structure proposed in this paper at first glance, but actually they are quite different. The fiber structure in [21] seems to be too much pursuit of the circular symmetry. For the fiber structure proposed in [21], the sizes of the air-holes in the ring structure of the cladding area are different in order to keep the same number of air-holes in different rings, so the air-holes in the inner ring are much smaller than those in the outer ring. Such structure with different hole size is more difficult to be fabricated than the structure we proposed and does not show better performance than the one proposed in this paper. We

* Corresponding author at: Beijing University of Posts and Telecommunications, State Key Laboratory of Information Photonics and Optical Communications, Xitucheng Rd., Beijing 100876, China.
E-mail address: xgzhang@bupt.edu.cn (X. Zhang).

http://dx.doi.org/10.1016/j.yofte.2016.07.009
1068-5200/

find that the proposed C-PCF in this paper possesses enough circular symmetry to ensure the stable transmission of OAM modes. The all-silica Bragg fibers which have been successfully fabricated in [22] proved that the fabrication of our new C-PCF is possible.

In Section 2, the structure of proposed C-PCF will be described. In Section 3, the mode features such as mode distribution, effective refractive index, chromatic dispersion, confinement loss, effective mode area, nonlinear coefficient, and modal birefringence will be discussed.

2. Design of the proposed circular photonic crystal fiber

The idea that C-PCF could be chosen as an OAM mode transmission fiber is as follows. The original base of the PCF is shown in Fig. 1(a). With the idea that OAM modes can propagate in a ring area, we change the core and the first air-hole ring into a large air hole in the center, and remove the second air-hole ring as the transmission region of OAM modes, leaving the rest air-hole rings as the part of the cladding. The final designed C-PCF is shown in Fig. 1(b). The background material of the designed fiber is silica with a refractive index of 1.444. The adjustable parameters of this structure include: the radius of the center air hole r, the inner radius of the cladding R, the diameters of the outer air holes d_n (n = 3,4,5...), the distance between two consecutive circles Λ and the number of outer air hole rings N. In this paper, we set that r = 4.4 μm, R = 6 μm, Λ = 2.2 μm, N = 4, d_n/Λ = 0.8 and $d_3 = d_4 = d_5 = d_6$ = 1.76 μm.

3. The OAM modes supported and their features

3.1. The OAM modes supported

The OAM states are formed by the linear combinations of the conventional vector eigenmodes of a fiber, and the formulas are [10]

$$\begin{cases} \mathrm{OAM}^{\pm}_{\pm l,m} = \mathrm{HE}^{\mathrm{even}}_{l+1,m} \pm j\mathrm{HE}^{\mathrm{odd}}_{l+1,m} \\ \mathrm{OAM}^{\mp}_{\pm l,m} = \mathrm{EH}^{\mathrm{even}}_{l-1,m} \pm j\mathrm{EH}^{\mathrm{odd}}_{l-1,m} \end{cases} \quad (1)$$

In this paper, we have analyzed the mode properties of the proposed C-PCF by using numerical simulation (COMSOL). And the fiber can support 26 OAM modes over a 650 nm bandwidth from 1.25 to 1.9 μm, including $\mathrm{OAM}^{\pm}_{\pm1,1}\{\mathrm{HE}_{21}\}$, $\mathrm{OAM}^{\pm}_{\pm2,1}\{\mathrm{HE}_{31},\mathrm{EH}_{11}\}$, $\mathrm{OAM}^{\pm}_{\pm3,1}\{\mathrm{HE}_{41},\mathrm{EH}_{21}\}$,$OAM^{\pm}_{\pm4,1}\{\mathrm{HE}_{51},\mathrm{EH}_{31}\}$, $\mathrm{OAM}^{\pm}_{\pm5,1}\{\mathrm{HE}_{61},\mathrm{EH}_{41}\}$, $\mathrm{OAM}^{\pm}_{\pm6,1}\{\mathrm{HE}_{71},\mathrm{EH}_{51}\}$ and $\mathrm{OAM}^{\pm}_{\pm7,1}\{\mathrm{HE}_{81},\mathrm{EH}_{61}\}$. Fig. 2 shows the intensity distributions of the vector eigenmodes supported by the proposed C-PCF. We can see that all the modes are well limited in the annular region.

3.2. Effective refractive index

The effective index of each vector mode as a function of wavelength by numerical simulation is shown in Fig. 3(a). We can see that the cut-off frequencies of HE_{91} and EH_{71} modes are about 1.5 μm (indicated by the open circle marks), so we ignore these two modes. To support OAM modes, the effective index separation between the vector modes must be larger than 1×10^{-4}, otherwise they will couple into LP modes. Fig. 3(b) shows the absolute value of effective index difference between HE and EH modes in the designed C-PCF. At the same time, we make a reference line of 1×10^{-4} in the same figure. From Fig. 3(b) we can see that the effective index differences of all HE and EH mode groups are larger than 1×10^{-4}, so all those modes can exist in the C-PCF in a stable manner.

3.3. Dispersion properties

The chromatic dispersion can be described as [23]

$$D = -\frac{\lambda}{c}\frac{d^2\mathrm{Re}[n_{\mathrm{eff}}]}{d\lambda^2} \quad (2)$$

In this work, the material dispersion is also taken into account. Fig. 4 shows the dispersion as a function of wavelength for different modes in the designed C-PCF. The figure shows that the dispersion variation for the OAM modes with $|l| \leqslant 4$ (l is the order of OAM mode) is within 39.84 ps/nm/km over a 750 nm bandwidth from1.25 to 2 μm, which is much more flattened than the results shown in [18]. And we can see that the dispersion variation of EH modes is less than HE modes. The dispersion variations of EH_{41}, EH_{51} and EH_{61} are: 36.68 ps/nm/km, 43.53 ps/nm/km and 46.1 ps/nm/km, and they are also less than the results shown in [18].

3.4. Confinement loss

The confinement loss for the proposed fiber structures has been calculated through [23]

$$L = \frac{2\pi}{\lambda}\frac{20}{\ln(10)}10^6\mathrm{Im}(n_{\mathrm{eff}})(dB/m) \quad (3)$$

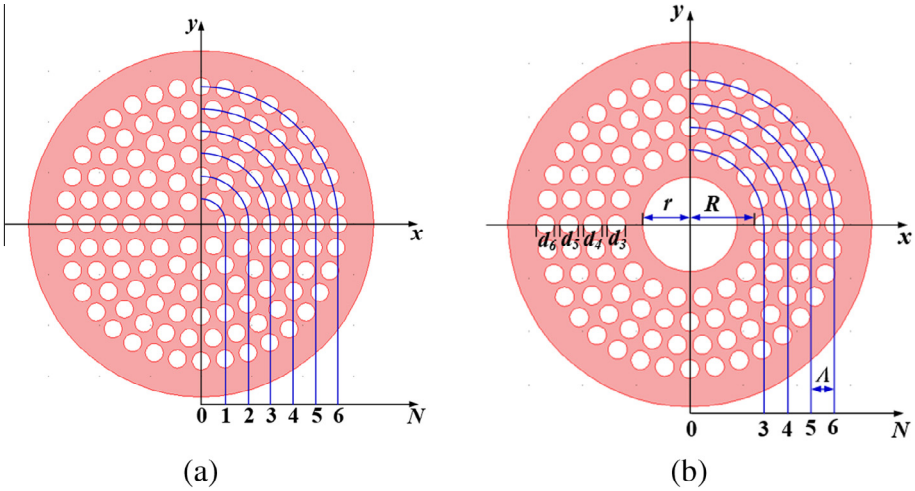

Fig. 1. (a) Cross-section of the original base of the PCF and (b) the new designed C-PCF.

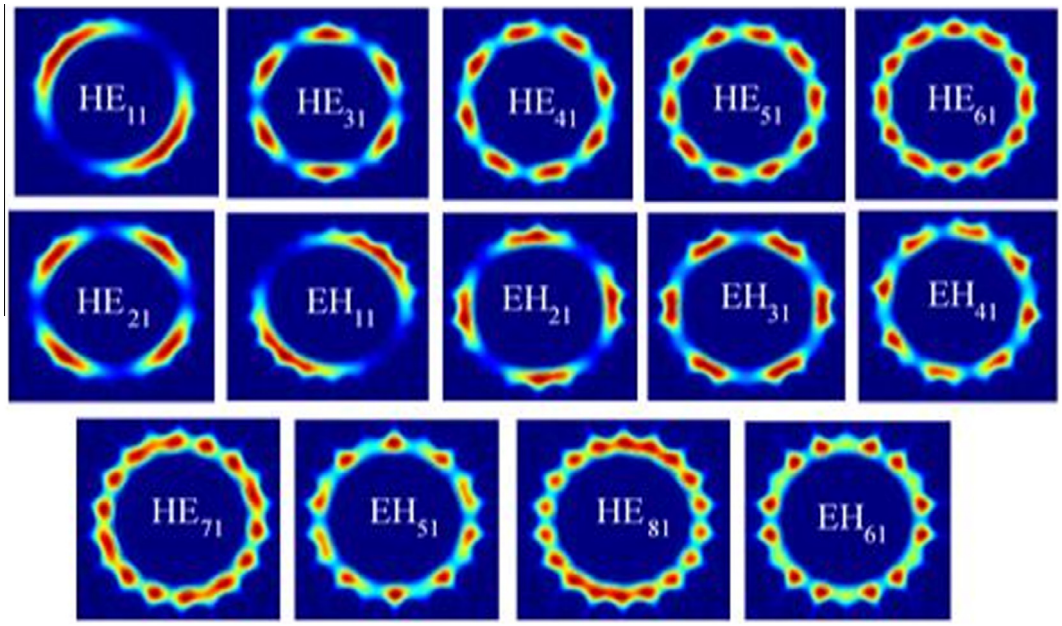

Fig. 2. The intensity distributions of the vector eigenmodes supported by the proposed C-PCF.

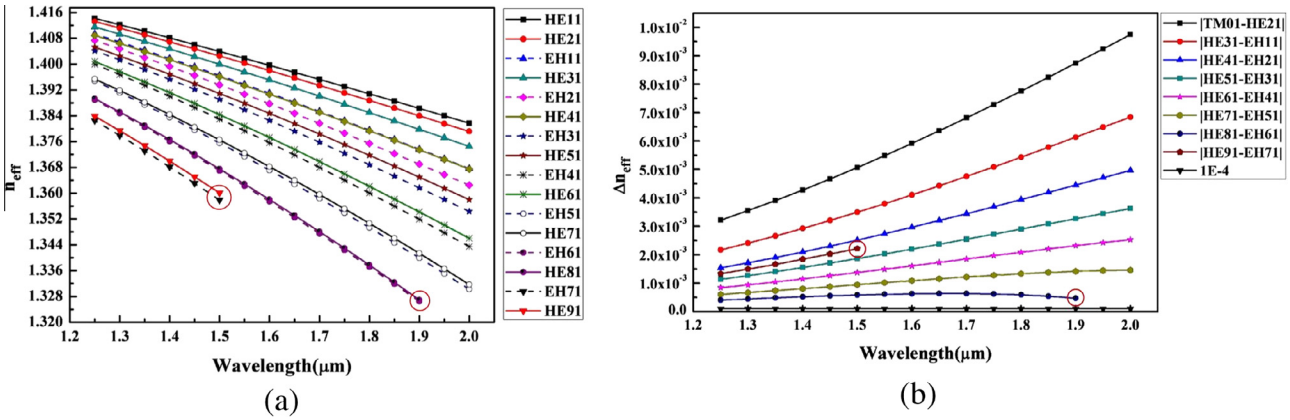

Fig. 3. (a) Effective refractive indices as a function of wavelength for different modes, and (b) the absolute value of effective index difference between HE and EH modes as a function of wavelength in the designed C-PCF.

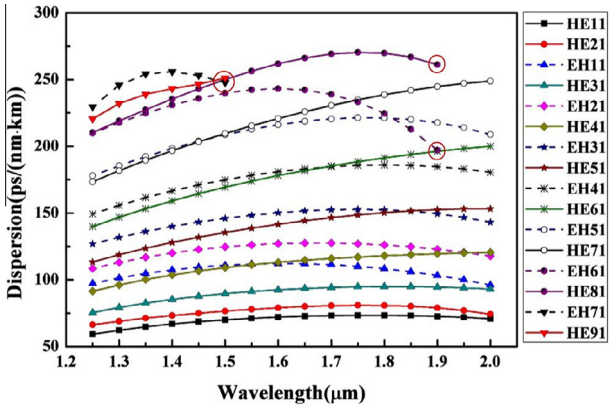

Fig. 4. Dispersion as a function of wavelength for different modes in the designed C-PCF.

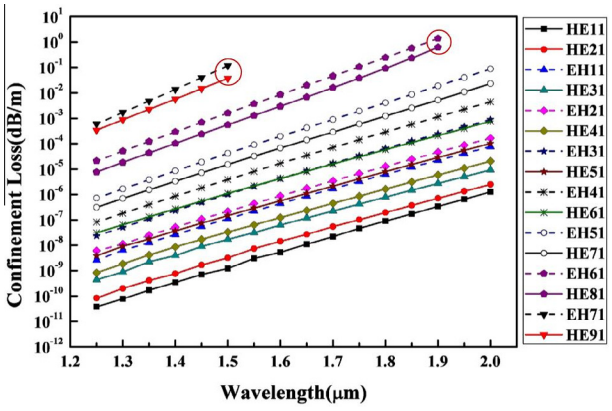

Fig. 5. Confinement loss as a function of wavelength for different modes in the designed C-PCF.

The confinement losses of all modes supported in the designed C-PCF are shown in Fig. 5. It shows that the confinement loss increases with the increasing of OAM mode order because of the more chance of leakage through the cladding for larger wavelength. For HE_{21} mode, the confinement loss is about 2.504×10^{-6} dB/m at 2 μm, which is lower about 4 orders of

magnitude than the results in[18]. The figure also shows that the confinement loss of EH modes is higher than that of HE modes. At 1.55 μm, the highest confinement loss belongs to EH_{61} mode, and it is about 0.003 dB/m.

3.5. Effective mode area and nonlinear coefficient

The effective mode area A_{eff} is calculated using its standard definition [24]

$$A_{eff} = \frac{\left(\int\int |\mathbf{E}(x,y)|^2 dxdy\right)^2}{\int\int |\mathbf{E}(x,y)|^4 dxdy} \tag{4}$$

where $\mathbf{E}(x,y)$ is the electrical field distribution of the transverse field. The nonlinear coefficient can be calculated by [24]

$$\gamma = \frac{2\pi n_2}{\lambda A_{eff}} \tag{5}$$

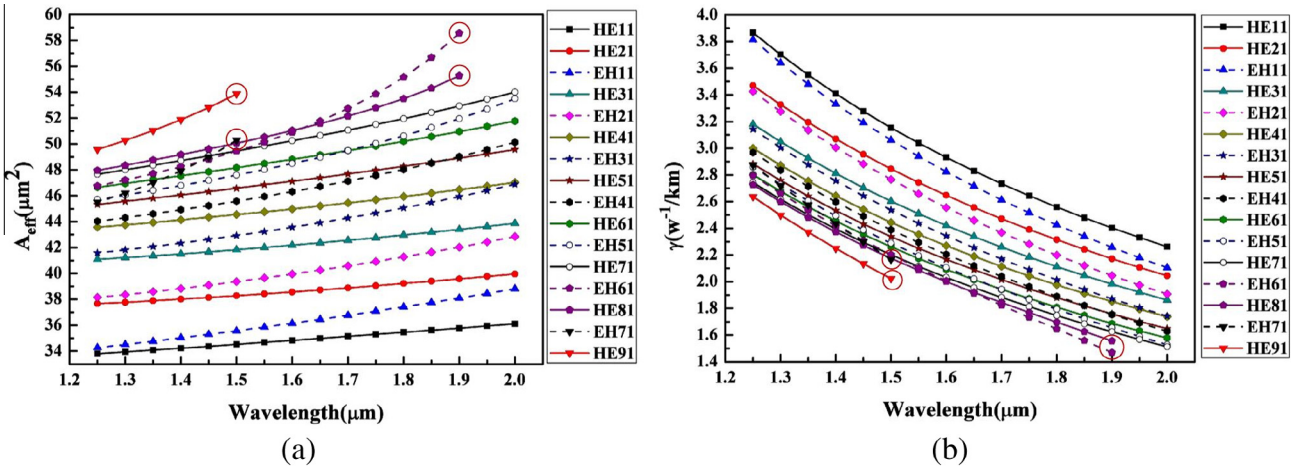

Fig. 6. (a) Effective mode area and (b) nonlinear parameter as a function of wavelength for different modes in the designed C-PCF.

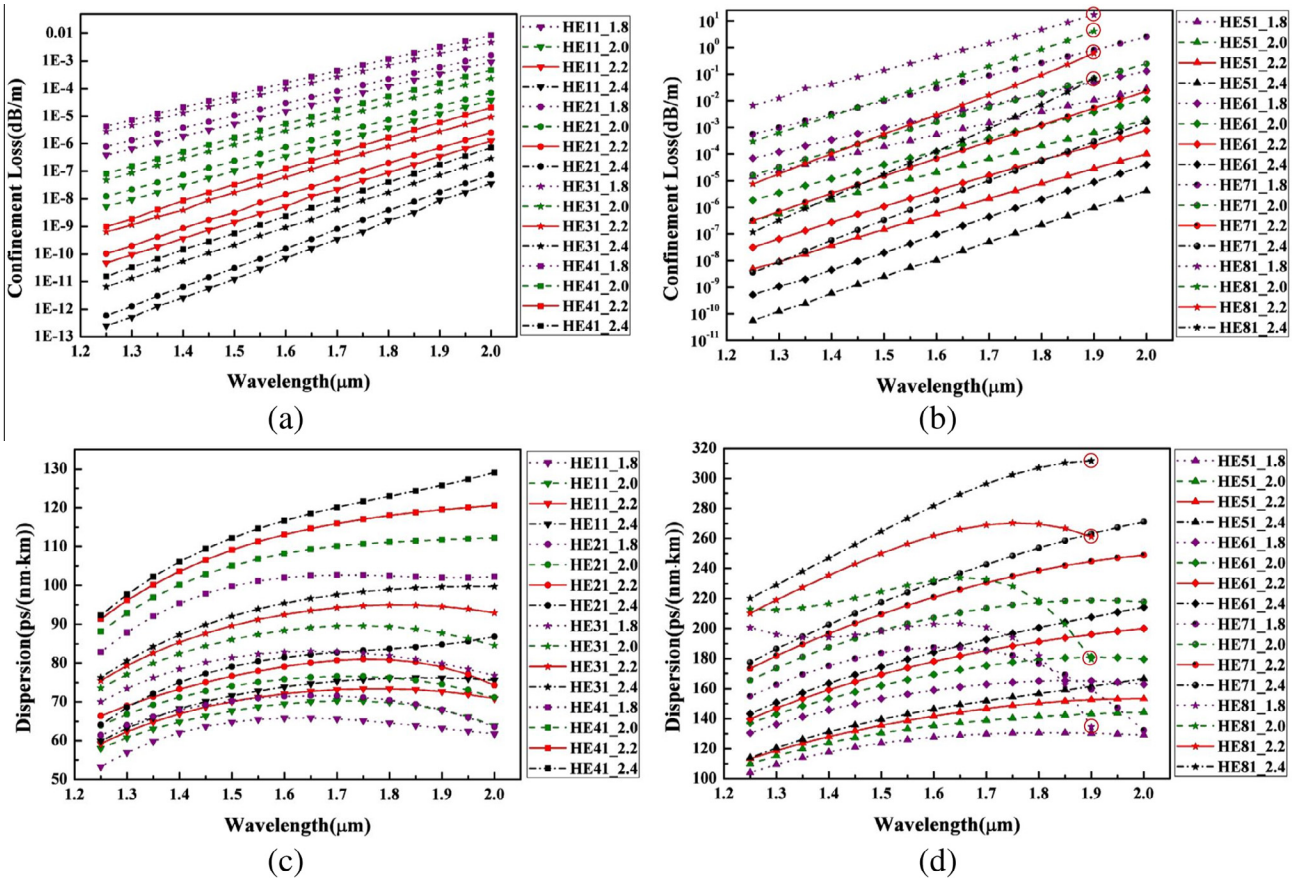

Fig. 7. (a, b) The confinement loss and (c, d) dispersion of all HE modes supported in the designed C-PCF for different Λ with r = 4.4 μm, R = 6 μm. The same modes are marked with the same symbol, and different colors and line styles represent different values of Λ.

where $n_2 = 2.6 \times 10^{-20}$ m^{2}W^{-1} is the nonlinear index for fused silica.

The effective mode area of the designed C-PCF is calculated by the full-vector finite element mode solver, and Fig. 6(a) shows the results. In Fig. 6(a), the effective mode area increases with the increasing of wavelength and mode order. And the nonlinear coefficient which is shown in Fig. 6(b) has opposite variation trends compared to the case of effective mode area. At 1.55 μm, the maximum of the effective mode area is 50.54 μm^2 (HE_{81}), and its nonlinear coefficient is the minimum (2.08 W^{-1}/km).

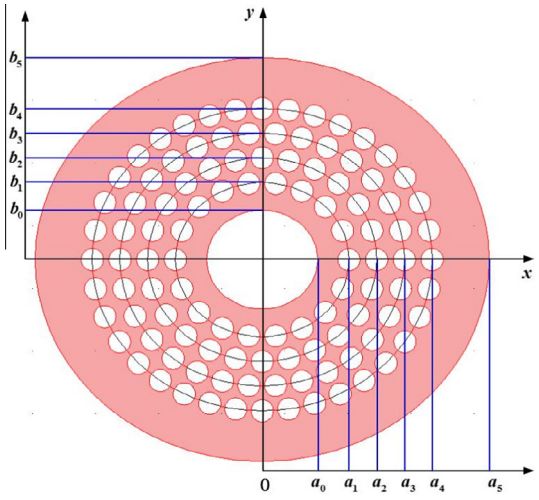

Fig. 8. Cross-section of the deformed C-PCF.

3.6. The influences of the fiber parameters on the confinement loss and dispersion

For the proposed fiber, we find that r can be set from 3.8 to 4.7 μm with other parameters unchanged. When r is smaller than 3.8 μm, the un-desired second-order radial modes will appear. On the contrary, when r is larger than 4.7 μm, the fiber will not support so many modes any more. In this work we set r = 4.4 μm.

We have also calculated the confinement loss and dispersion for all HE modes at Λ = 1.8 μm, 2.0 μm, 2.2 μm, 2.4 μm, respectively. Fig. 7 shows the results. We use different colors and line styles to represent different consequences for different Λ, and the same modes are marked with the same symbol. From Fig. 7(a) and (b) we can see that the confinement loss decreases with the increasing of Λ for all modes. And for the same mode, the confinement loss changes several orders of magnitude for different Λ. Fig. 7 (c) and (d) shows the trend that the dispersion and its variation increase with the increasing of Λ. But the changes for the variation of dispersion under the influence of Λ are not very large. Compare the confinement loss with the dispersion, we can see that the change of Λ has a larger influence on the confinement loss than the dispersion. It seems that the propagation characteristics of the structure, in which Λ = 2.4 μm, is better. But when Λ = 2.4 μm, the distance of two adjacent air holes in the first

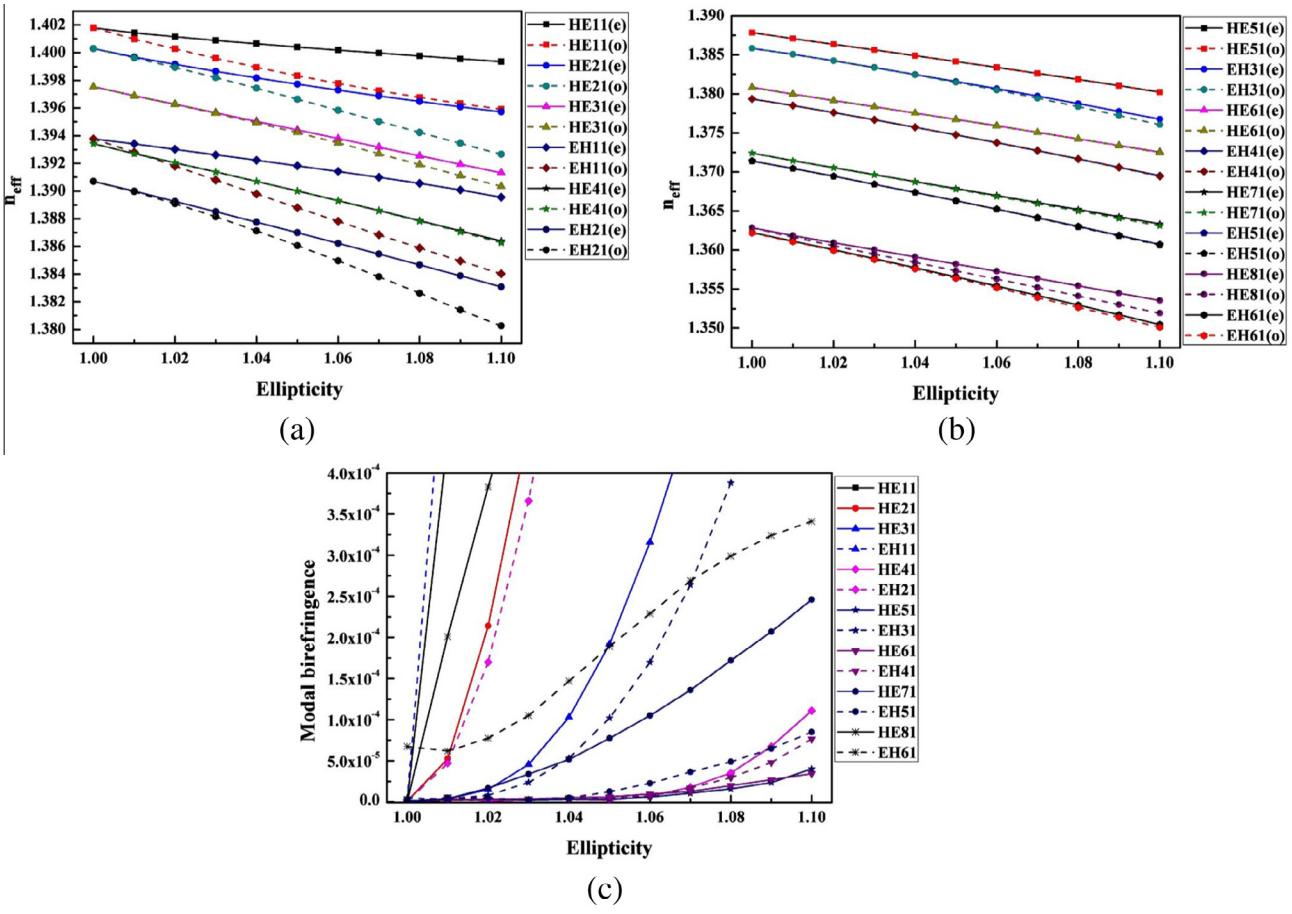

Fig. 9. (a, b) Effective refractive indices of all even and odd modes for the vector modes supported in the C-PCF and (c) the modal birefringence of the vector modes as a function of the ellipticity at 1.55 μm.

cladding ring is too close to be manufactured. Therefore, we set Λ = 2.2 μm for the reason of trade-off in this work.

3.7. Modal birefringence

The modal birefringence is also a parameter to reflect the performance of the OAM mode supported fiber. The modal birefringence is defined as[17]

$$B_m = |n_{\text{eff}}^{\text{even}} - n_{\text{eff}}^{\text{odd}}| \quad (6)$$

where $n_{\text{eff}}^{\text{even}}$ and $n_{\text{eff}}^{\text{odd}}$ are the effective refractive indices of the even and odd eigenmodes that compose the OAM modes.

Here we limit our discussion in the fabrication tolerance for the designed C-PCF fiber. In other word, the geometric deformation here is limited to be induced by an imperfect fabrication. For simplicity, we suppose that the central air hole and all outer rings keep the same ellipticity ε when the fiber is deformed, while all the outer air holes are still circle, as shown in Fig. 8, for the reason that for the small holes in outer ring, there exist surface tension that tends to keep the small holes in their original shapes. The minor axis values which measure the distances between the central air hole and all outer rings can be counted by $b_n = \frac{a_n}{\varepsilon}(n = 0, 1, 2, \ldots 5)$.

Fig. 9(a) and (b) shows the effective refractive indices of all even and odd modes for the vector modes supported in the C-PCF as a function of the ellipticity at 1.55 μm. It shows that the difference of effective refractive indices between even and odd modes for the same HE or EH mode increases with the increasing of the ellipticity. Make the comparison of Fig. 9(a) and (b), we can find that most of higher order modes have a smaller difference than the lower order modes. Fig. 9(c) shows the modal birefringence of the vector modes as a function of the ellipticity at 1.55 μm, and it verifies this conclusion. From Fig. 9(c) we can see that there will be a large modal birefringence for EH_{11}, HE_{11}, HE_{81}, HE_{21} and EH_{21} modes when the ellipticity is larger than 1. While the modal birefringence of HE_{41}, HE_{51}, HE_{61}, EH_{41} and EH_{51} modes keep relatively small values even the ellipticity is up to 1.08. So these modes may keep their good performances when the ellipticity is less than 1.08.

4. Conclusion

We have proposed a new circular photonic crystal fiber which can stably support 26 OAM modes from1.25 to 1.9 μm (650 nm) with large enough effective index separations. The numerical analysis shows that the proposed fiber possesses very good fiber features, such as low confinement loss which is lower than 0.003 dB/m at wavelength of 1.55 μm, flat chromatic dispersion whose dispersion variation for the OAM modes with $|l| \leqslant 4$ is within 39.84 ps/nm/km over a 750 nm bandwidth from1.25 to 2 μm, and small nonlinear coefficient which is less than 2.08 W^{-1}/km for all modes at 1.55 μm. In addition, the influence of geometric deformation on the modal birefringence of the proposed fiber has also been discussed. It is proved that the modal birefringence caused by the geometric deformation is different for different vector modes, and most of the higher order modes have a smaller modal birefringence than the lower order modes when the deformation is not very severe. Based on the flexibility of the structure, we can obtain a new C-PCF with a set of good features by adjusting the parameters. In a word, this kind of fiber structure will be a promising candidate for OAM based mode division multiplexing in fiber transmission systems.

Acknowledgments

This work was supported by the National Natural Science Foundation of China, China (Grant No. 61571057, 61501214).

Appendix A. Supplementary data

Supplementary data associated with this article can be found, in the online version, at http://dx.doi.org/10.1016/j.yofte.2016.07.009.

References

[1] L. Allen et al., Orbital angular momentum of light and transformation of Laguerre Gaussian Laser modes, Phys. Rev. A 45 (11) (1992) 8185–8189.
[2] J. Wang et al., Terabit free-space data transmission employing orbital angular momentum multiplexing, Nat. Photonics 6 (7) (2012) 488–496.
[3] B. Nenad et al., Terabit-scale orbital angular momentum mode division multiplexing in fibers, Science 340 (6140) (2013) 1545–1548.
[4] H. Hao et al., 100 Tbit/s free-space data link enabled by three-dimensional multiplexing of orbital angular momentum, polarization, and wavelength, Opt. Lett. 39 (2) (2014) 197–200.
[5] W. Jian et al., Ultra-high 435-bit/s/Hz spectral efficiency using N-dimensional multiplexing and modulation link with pol-muxed 52 orbital angular momentum (OAM) modes carrying Nyquist 32-QAM signals, in: European Conference on Optical Communication (ECOC), 2015, 2015.
[6] H.I. Sztul et al., Cylindrical vector beam generation from spun fiber, Proceedings of SPIE – The International Society for Optical Engineering 7227 (5) (2009) 561–564.
[7] N. Bozinovic, P. Kristensen, S. Ramachandran, Long-range fiber-transmission of photons with orbital angular momentum, in: Conference on Lasers and Electro-Optics (CLEO), 2011, 2011.
[8] N. Bozinovic, P. Kristensen, S. Ramachandran, Are orbital angular momentum (OAM/Vortex) States of light long-lived in fibers?, Frontiers in Optics 2011/Laser Science XXVII, Optical Society of America, San Jose, California, 2011
[9] Y. Yue et al., Mode properties and propagation effects of optical Orbital Angular Momentum (OAM) modes in a ring fiber, IEEE Photonics J. 4 (2) (2012) 535–543.
[10] C. Brunet et al., Design, fabrication and validation of an OAM fiber supporting 36 states, Opt. Express 22 (22) (2014) 26117–26127.
[11] P. Gregg et al., Stable transmission of 12 OAM states in air-core fiber, in: Conference on Lasers and Electro-Optics (CLEO), 2013, 2013.
[12] J. Ye et al., Excitation and separation of vortex modes in twisted air-core fiber, Opt. Express 24 (8) (2016) 8310–8316.
[13] B. Ung et al., Few-mode fiber with inverse-parabolic graded-index profile for transmission of OAM-carrying modes, Opt. Express 22 (15) (2014) 18044–18055.
[14] S. Li, J. Wang, A compact trench-assisted multi-orbital-angular-momentum multi-ring fiber for ultrahigh-density space-division multiplexing (19 rings × 22 modes), Sci. Rep. 4 (2014) (3853-3853).
[15] L. Shuhui, W. Jian, Supermode fiber for orbital angular momentum (OAM) transmission, Opt. Express 23 (14) (2015) 18736–18745.
[16] B.U. Charles Brunet, Bélanger Pierre-André, Messaddeq Younès, L.A.R. Sophie LaRochelle, Vector mode analysis of ring-core fibers: design tools for spatial division multiplexing, J. Lightwave Technol. 32 (23) (2014).
[17] M. Zhu et al., A new designed dual-guided ring-core fiber for OAM mode transmission, Opt. Fiber Technol. 25 (2015) 58–63.
[18] Y. Yue et al., Octave-spanning supercontinuum generation of vortices in a As2S3 ring photonic crystal fiber, in: Conference on Lasers and Electro-Optics (CLEO), 2012, 2012.
[19] C. Zhao et al., Design of multicore photonic crystal fibers to generate cylindrical vector beams, J. Lightwave Technol. 34 (4) (2016) 1206–1211.
[20] X.M. Xi et al., Orbital-angular-momentum-preserving helical Bloch modes in twisted photonic crystal fiber, Optica 1 (3) (2014) 165–169.
[21] G. Zhou et al., Design and analysis of a microstructure ring fiber for orbital angular momentum transmission, IEEE Photonics J. 8 (2) (2016) 1–12.
[22] G. Vienne et al., Ultra-large bandwidth hollow-core guiding in all-silica Bragg fibers with nano-supports, Opt. Express 12 (15) (2004) 3500–3508.
[23] P.S. Maji, P.R. Chaudhuri, Circular photonic crystal fibers: numerical analysis of chromatic dispersion and losses, ISRN Opt. 2013 (2013) 1–9.
[24] H. Xu et al., Ultra-flattened chromatic dispersion control for circular photonic crystal fibers, J. Opt. 13 (5) (2011) 994–1001.